CrossMark

ORIGINAL ARTICLE

Orbital malignant lesions in adults: multiparametric MR imaging

Bo Sun[1,2] · Liyuan Song[2]

Abstract

Purpose To assess the benefit of combining diffusion-weighted imaging and dynamic contrast-enhanced (DCE) MR imaging in the preoperative evaluation of orbital lymphoma and other malignancies in adults.

Materials and methods This retrospective study was institutional review board-approved and informed consent was waived. Pretreatment MR imaging was performed in 52 patients with malignant orbital lesions. Apparent diffusion coefficient (ADC) and DCE MR parameters were evaluated in 30 patients with orbital lymphoma and 22 patients with other orbital malignancies. Independent-samples t-test or Wilcoxon rank-sum test was used to compare parameters. The diagnostic capability was evaluated by using receiver operating characteristic curve (ROC) analysis.

Results Lymphoma demonstrated significantly lower mean ADC ($P < 0.001$), T_{max} ($P = 0.001$), enhancement ratio (ER) ($P < 0.001$), contrast index (CI) ($P < 0.001$) and significantly higher washout ratio (WR) ($P = 0.002$) than other malignancies in the orbit. ROC analysis indicated that T_{max} alone or a combination with ADC and ER showed the optimal sensitivity (96.67%), a combination of ADC and WR showed optimal specificity (95.45%), while a combination of ADC and ER showed optimal accuracy (90.38%) in differentiating lymphoma from other malignancies.

Conclusion Multiparametric MRI can help to differentiate orbital lymphoma and other malignancies.

✉ Bo Sun
  sunbo-china@163.com

1   Department of Radiology, Harbin Shi Di Yi Yi Yuan,
    Harbin 150010, China

2   Department of Radiology, Capital Medical University Beijing
    Tongren Hospital, Beijing, China

Introduction

Malignant orbital lesions present with a broad spectrum of diseases: lymphoma, malignant epithelial tumors; carcinoma and malignant connective tissue tumors; or sarcoma [1–3]. Orbital lymphoma is treated with low-dose radiation therapy [4], whereas surgery and postoperative radiation therapy are commonly used as initial local treatment for other malignancies in the orbit [5].

Diffusion-weighted (DW) imaging and dynamic contrast-enhanced (DCE) magnetic resonance (MR) imaging have been used for preoperative evaluation of space-occupying lesions in the orbit and both of them have proved to be valuable in differential diagnosis [1, 3, 6–16]. DW imaging has made it possible to distinguish orbital lymphoma from other neoplastic and nonneoplastic orbital lesions [8] or orbital inflammation [1, 9, 15, 16]. DCE MR imaging shows high value in the characterization of orbital lesions [6, 11, 14–16]. Time intensity curve (TIC) patterns and TIC parameters prove to reflect the vascular physiology of orbital lymphoma [15, 16]. Furthermore, the combination of DW imaging and DCE MR imaging could increase the diagnostic performance of preoperative differentiation of orbital lesions in adults [14–16]. However, with regard to orbital lymphoma and other malignancies, the contributions of DCE MR imaging and the combined use of DW imaging and DCE MR imaging remain unclear.

Therefore, the purpose of our study was to compare the diagnostic performance of DW imaging, DCE-MR

imaging, and both techniques combined for detection of lymphoma from other malignancies in the orbit.

Materials and methods

Study population

Our institutional review board approved this retrospective study and waived the informed consent requirement. From a retrospective review of the database of our institution during the period from 2013 to 2016, we identified 52 patients according to the following inclusion and exclusion criteria. The inclusion criteria for this study were: (a) patients underwent orbital MR imaging including DW imaging and DCE MR imaging before biopsy or surgery, (b) patients had no history of surgery or treatment in the affected orbit,

(c) malignant tumors were pathologic findings identified from biopsy or surgery, and (d) patients were adult (age ≥ 18). The exclusion criteria for this study were as follows: (a) invasion into orbit from its vicinity, such as the skull base, paranasal sinus or nasopharynx; or (b) lesions originating from eyelids or globe. There were 52 patients who were identified on the basis of the final diagnosis of orbital lymphoma or other malignancies: 27 men (mean age 50 years; age range 19–67 years) and 25 women (mean age 48 years; age range 19–68 years). The final diagnoses of these patients are shown in Table 1 and the locations are detailed in Table 2.

Imaging protocol

All patients underwent 3.0-T MR imaging (Signa HDxt scanner; GE Healthcare) with use of an eight-channel

Table 1 Diagnosis of 52 orbital malignant lesions and their index

Diagnosis of lesions (N)	ADC $\times 10^{-3}$ mm^2/s	TIC parameters			
		T_{max}	ER	CI	WR
Lymphoma (30)	0.694 ± 0.128	126.4 ± 49.6	0.908 ± 0.193	0.823 ± 0.199	0.098 ± 0.046
Mucosa-associated lymphoid tissue (MALT) (27)	0.701 ± 0.131	126.0 ± 51.8	0.901 ± 0.199	0.815 ± 0.204	0.100 ± 0.047
Diffuse large B-cell lymphoma (DLBCL) (2)	0.588 ± 0.021	118.0 ± 22.6	0.962 ± 0.191	0.865 ± 0.188	0.103 ± 0.017
Follicular lymphoma (1)	0.701	153	0.998	0.961	0.037
Other malignancies (22)	1.186 ± 0.315	207.0 ± 94.0	1.326 ± 0.372	1.265 ± 0.400	0.055 ± 0.071
Adenoid cystic carcinoma (10)	1.302 ± 0.292	264.1 ± 52.9	1.491 ± 0.292	1.467 ± 0.283	0.015 ± 0.024
Squamous cell carcinoma (3)	1.187 ± 0.129	106.3 ± 117.6	1.086 ± 0.039	0.957 ± 0.130	0.120 ± 0.099
Adenocarcinoma (3)	1.167 ± 0.439	224.7 ± 94.9	1.034 ± 0.394	1.003 ± 0.421	0.039 ± 0.036
Malignant melanoma (2)	0.953 ± 0.322	177.5 ± 122.3	1.324 ± 0.351	1.224 ± 0.447	0.088 ± 0.096
Rhabdomyosarcoma (1)	0.770	108.0	1.184	1.019	0.139
Myeloid sarcoma (1)	0.635	57.0	0.812	0.630	0.224
Chondrosarcoma (1)	1.250	230.0	2.142	2.076	0.031
Salivary duct carcinoma (1)	1.450	171.0	1.106	1.096	0.009

N is abbreviation for number

Table 2 Location of the tumors

Tumors	Intraconal	Extraconal	Lacrimal fossa	Anterior orbit preseptal
MALT	20	26	18	22
DLBCL	1	1	1	0
Follicular lymphoma	1	1	1	1
Adenoid cystic carcinoma	8	10	10	1
Squamous cell carcinoma	1	3	0	2
Adenocarcinoma	3	3	3	1
Malignant melanoma	2	1	0	0
Rhabdomyosarcoma	1	1	0	0
Myeloid sarcoma	1	1	0	1
Chondrosarcoma	1	0	0	0
Salivary duct carcinoma	1	1	1	1

high-resolution head coil. Our imaging protocol included axial fast spin echo (FSE) T1-weighted imaging (T1WI), axial FSE T2-weighted imaging (T2WI), and coronal FSE T1WI. The parameters were the following: T1WI: repetition time (TR), 400 ms; echo time (TE), 10 ms; T2WI: TR, 3000 ms; TE, 120 ms; number of excitations (NEX), 2; matrix, 384×256; field of view (FOV), 180×180 mm; section thickness, 3 mm; gap, 0.3 mm.

DW imaging

DW images were performed with echo planar imaging diffusion weighted imaging in the axial plane with fat suppression (TR 5000 ms, TE 64–77 ms; section thickness, 3 mm; gap, 0.3 mm; FOV, 160×160 mm; matrix, 128×128) sensitized to incoherent motion by a pair of gradient pulses. Two DW images were acquired with b values of 0, 1000 s/mm^2.

DCE MR imaging

DCE MR imaging was acquired by using a fast-spoiled gradient recalled (FSPGR) sequence. The detailed imaging parameters were as follows: TR/TE, 8.4/4 ms; 1 excitation; flip angle, 15°; and a slice thickness of 3.2 mm at 0 intervals. A total of 37 scans with 16 sections were obtained. Each scan took 9 s; and there was an interval of 0–2 s between scans. Total scanning time was 344 s. Injection of gadolinium-based MR contrast agents (Magnevist; Bayer Schering, Berlin, Germany) at a dose of 0.1 mmol per kg of body weight was administered intravenously by using a power injector (Spectris Solaris; Medrad, Indianola, Pennsylvania) at a flow rate of 2 ml/s.

After obtaining DCE MR imaging data, axial, coronal, and oblique sagittal FSE T1WI was performed. Axial T1WI used fat suppression. The parameters of the pre-contrast sequence were also used in these sequences.

Imaging analysis

Two experienced head and neck radiologists (with 6 and 4 years of experience), who were blinded to diagnosis, reviewed all MR image sets, and selected a region of interest (ROI) for each study independently. DW imaging and DCE MR imaging were evaluated with a GE ADW 4.4 work-station (GE Healthcare, Milwaukee, Wisconsin) with functool 2 software.

The radiologists selected the affected side for ROI; when both sides were affected, we selected the side where the biopsy was conducted.

For DW imaging analysis, by using T2WI and contrast-enhanced axial images as a reference, the ROI was drawn manually to include the entire lesion on the apparent

diffusion coefficient (ADC) map. Care was taken to avoid cystic, necrotic and hemorrhagic portions of the lesion that might influence the ADC value. Cystic components were hyperintense areas on T2WI. Necrotic components were the interior non-enhancing part on contrast-enhanced axial images. Hemorrhagic lesions were rare in the orbital lesions. To standardize the image analysis as much as possible, lesion ADC was measured in the section without the infiltrated extraocular muscles or optic nerve for reduction of the impact of normal tissue; strict attention was paid to normal lacrimal gland so that it was not included in ROI delimitation in some lesions; the edges of each lesion were excluded to reduce the partial volume effect; distortion artifacts were also carefully avoided from ROI delimitation.

For DCE MR imaging analysis, the ROI was placed in the same location as for DW imaging. A TIC was then generated. The signal intensity (SI) was calculated from the mean pixel value on each acquired dynamic image.

1. SI_{pre} was the baseline signal intensity (SI corresponding to time $T = 0$) and SI_{max} was the maximal signal intensity over the entire DCE MR imaging series. T_{max} was measured from the time of arrival to peak time (T_{max} = peak time − $T1$. Peak time was the time corresponding to the SI_{max}). The enhancement ratio (ER) was calculated from ER = $(SI_{max} - SI_{pre})/SI_{pre}$ [6, 11, 15–20].
2. SI_{end} was the final signal intensity over the entire DCE MR imaging series. Contrast index (CI) and washout ratio (WR) were calculated by using the following formulae, CI = $(SI_{end} - SI_{pre})/SI_{pre}$ or WR = $(SI_{max} - SI_{end})/(SI_{max} - SI_{pre})$ [6, 11, 15–20].

Statistical analysis

Continuous variables were expressed as the mean ± standard deviation. The normality for any continuous variable was examined by using a Kolmogorov–Smirnov Z test. For normally distributed variables, an independent t-test was performed to examine the group effect. For variables that were not normally distributed, the Wilcoxon rank-sum test was used.

Receiver operating characteristic curve (ROC) analysis was performed to determine a cutoff value to predict lymphoma. Binary logistic regression analysis calculated the predicted probability of combination of ADC and DCE MR imaging parameters, then ROC analysis was performed to assess the diagnostic value of combined indexes.

To assess the reliability of measurements between radiologists, the interobserver variability was evaluated by using the intraclass correlation coefficient (ICC).

All tests were two-sided, and $P < 0.05$ was considered indicative of a significant difference. All statistical analyses were performed by using commercially available statistical software (SPSS for IBM, version 18.0, Chicago, IL, USA).

Results

DW imaging results

The lymphoma showed significantly lower mean ADC ($0.694 \pm 0.128 \times 10^{-3}$ mm^2/s) (Fig. 1) than other malignancies ($1.186 \pm 0.315 \times 10^{-3}$ mm^2/s) (Fig. 2) ($t = 6.920$, $P < 0.001$) (Table 3) (Fig. 3). By applying an ADC cutoff value of 0.888×10^{-3} mm^2/s, the sensitivity (predicting lymphoma), specificity (predicting other malignancies), and diagnostic accuracy were 93.33, 81.82 and 88.46%, respectively (Table 3; Fig. 4), with an area under the ROC curve (AUC) of 0.912 [95% confidence interval (CI) 0.828, 0.996].

DCE MR imaging results

Distribution of T_{max}, ER, CI and WR between lymphoma and other malignancies is detailed in Table 3. All of them showed significant difference between lymphoma and other malignancies ($P = 0.001$, $P < 0.001$, $P < 0.001$, and $P = 0.002$, respectively) (Figs. 1, 2, 3).

Cutoff value, AUC, sensitivity (predicting lymphoma), specificity (predicting other malignancies) and accuracy of T_{max}, ER, CI and WR are detailed in Table 4 (Fig. 4).

Combination of DW imaging and DCE MR imaging

With binary logistic regression analysis and ROC analysis, sensitivity (predicting lymphoma), specificity (predicting other malignancies) and accuracy of ADC combined with T_{max} were 93.33, 81.82 and 88.46%, respectively, with AUC of 0.923 (95% CI 0.846, 0.999); of ADC combined with ER were 96.67, 81.82 and 90.38%, respectively, with AUC of 0.917 (95% CI 0.823, 1.000); of ADC combined with CI were 93.33, 81.82 and 88.46%, respectively, with AUC of 0.914 (95% CI 0.827,
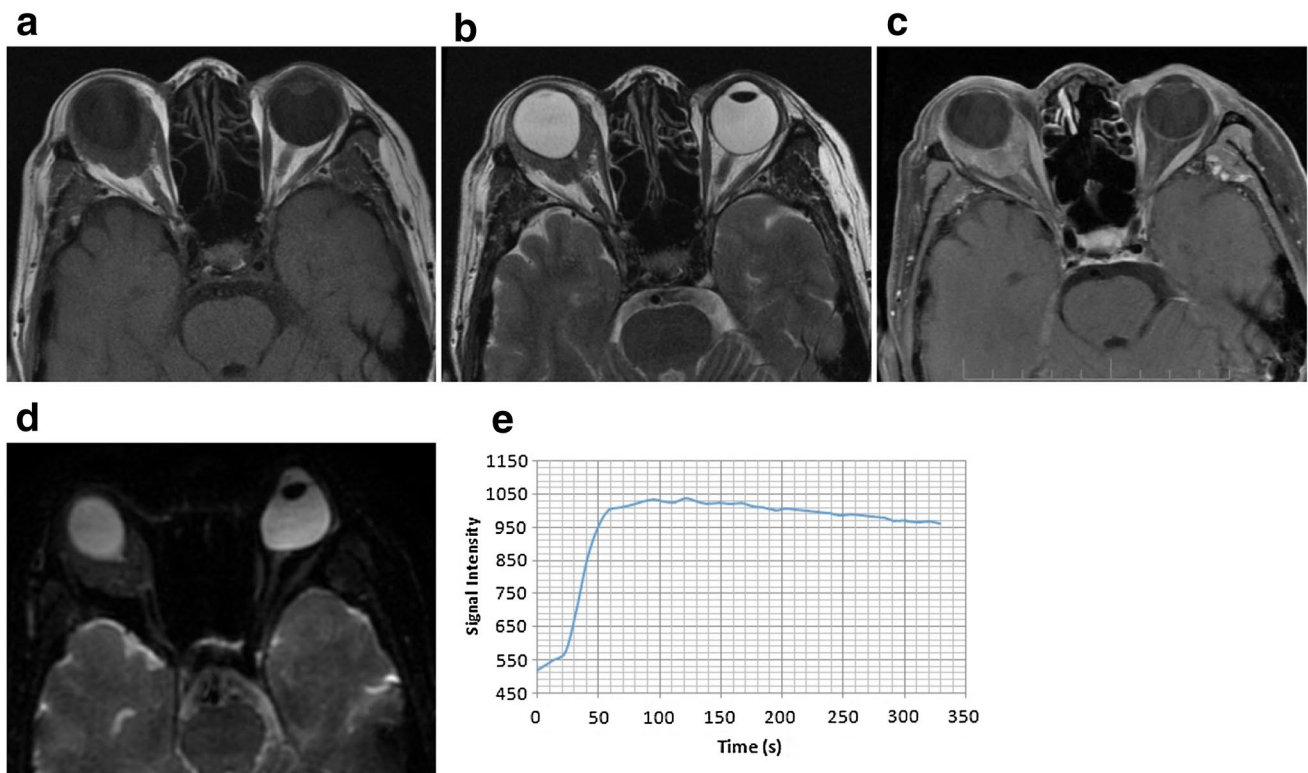

Fig. 1 MR images in 60-year-old woman with lymphoma identified a well-defined mass molding around globe in the right intraconal space. **a** T1WI showed a homogeneously isointense mass. **b** T2WI showed a homogeneously isointense mass. **c** T1-weighted fat-suppressed post-contrast imaging shows mildly homogeneous enhancement of the mass. **d** DWI shows homogeneous isointensity with ADC $= 0.672 \times 10^{-3}$ mm^2/s. **e** Time–intensity curve for this patient was characterized as a plateau pattern with $T_{max} = 122$ s, ER $= 0.7914$, CI $= 0.6930$ and WR $= 0.1243$
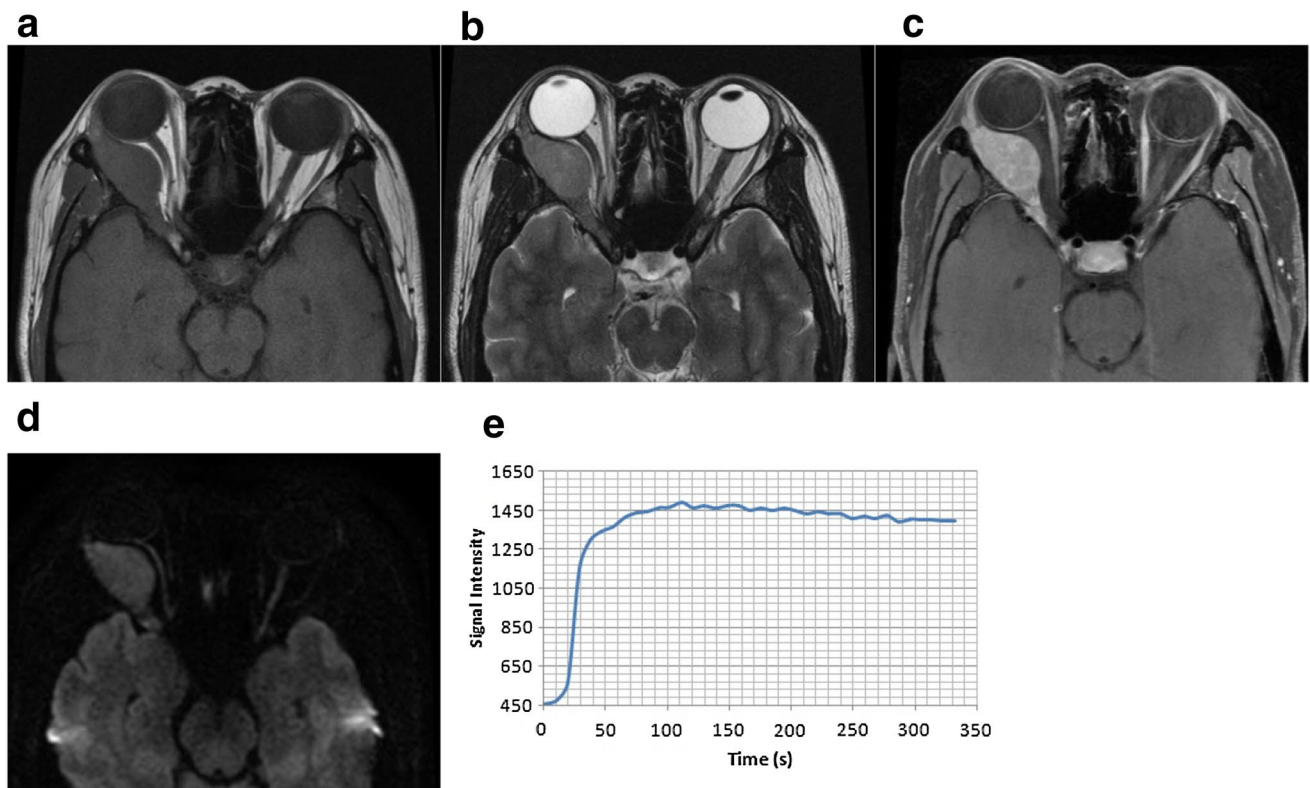
Fig. 2 MR images in a 45-year-old woman with adenoid cystic carcinoma demonstrated an oval well-defined mass in the right intraconal space. **a** T1WI showed a homogeneously isointense mass. **b** T2WI showed a homogeneously hyperintense mass. **c** T1-weighted fat-suppressed post-contrast image shows moderate and homogenous enhancement. **d** DWI shows a slightly high signal with $ADC = 0.983 \times 10^{-3}$ mm^2/s. **e** Time–intensity curve for this patient was characterized as plateau pattern with $T_{max} = 121$ s, $ER = 1.6787$, $CI = 1.558$ and $WR = 0.0722$

Table 3 Differences of ADC and TIC parameters between lymphoma and other malignancies

Index	Lymphoma	Other malignancies	t or z value	P value	ICC
$ADC \times 10^{-3}$ mm^2/s	0.694 ± 0.128	1.186 ± 0.315	6.920 (t)	<0.001	0.966
T_{max}	126.4 ± 49.6	207.0 ± 94.0	3.667 (t)	0.001	0.927
ER	0.908 ± 0.193	1.326 ± 0.372	4.812 (t)	<0.001	0.912
CI	0.823 ± 0.199	1.265 ± 0.400	4.766 (t)	<0.001	0.925
WR	0.098 ± 0.046	0.055 ± 0.071	3.057 (z)	0.002	0.800

Data are means ± standard deviations

ADC, T_{max}, ER and CI demonstrated t value; while WR demonstrated z value

1.000); of ADC combined with WR were 80, 95.45 and 86.54%, respectively, with AUC of 0.939 (95% CI 0.872, 1.000) (Table 4) (Fig. 4).

ROC analysis indicated that T_{max} alone or a combination with ADC and ER showed the optimal sensitivity (96.67%), a combination of ADC and WR showed optimal specificity (95.45%), while a combination of ADC and ER showed optimal accuracy (90.38%) in differentiating lymphoma from other malignancies in the orbit.

Interobserver agreement

There was perfect agreement interobserver agreement for mean ADC ($k = 0.966$), T_{max} ($k = 0.927$), ER ($k = 0.912$), CI ($k = 0.925$) and WR ($k = 0.800$) (Table 3).
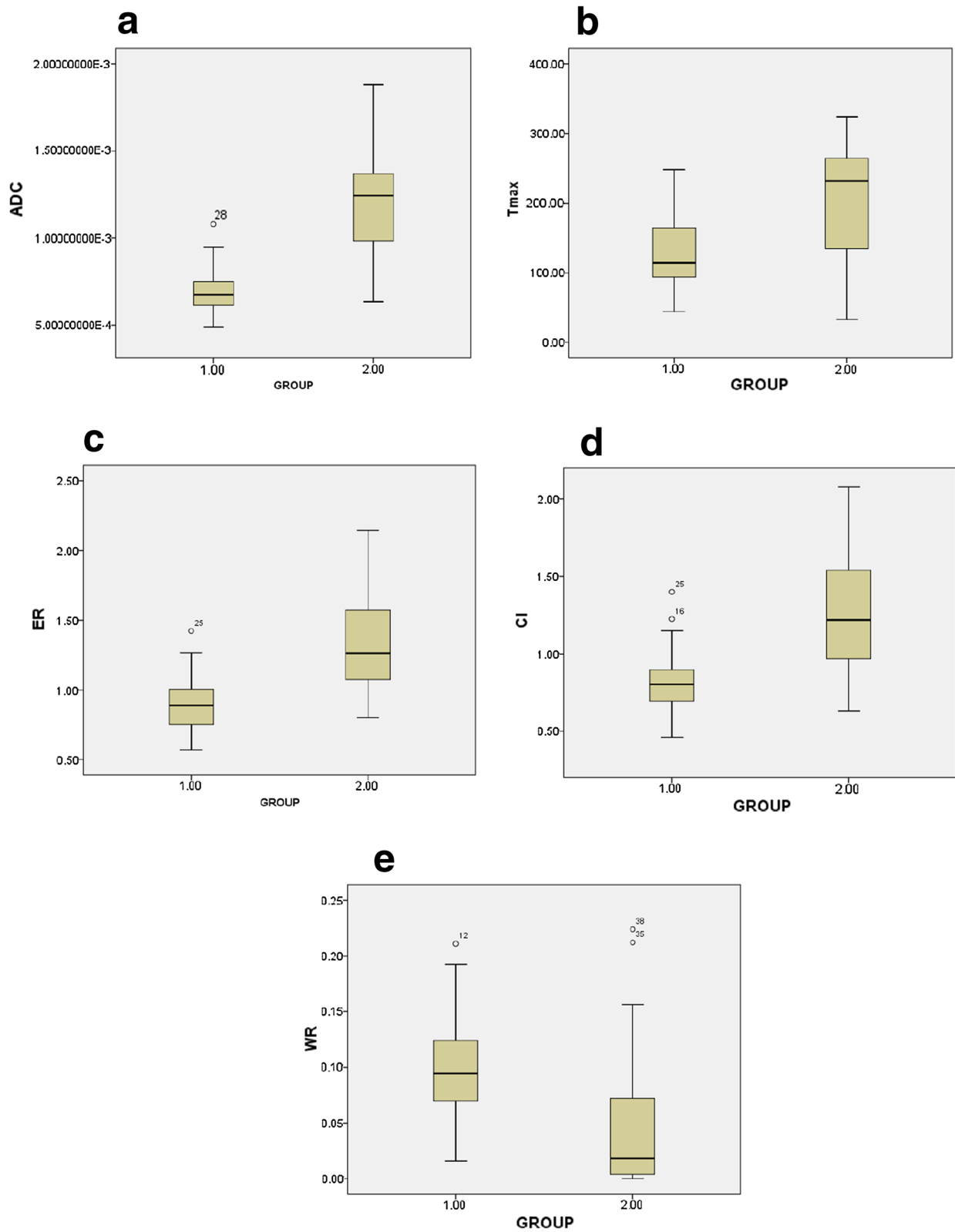
Fig. 3 Box-and-whisker plots show ADC (**a**), T_{max} (**b**), ER (**c**), CI (**d**) and WR (**e**) calculated for orbital lymphoma and carcinoma. The lymphoma showed significantly lower ADC, T_{max}, ER, CI, and sig-nificantly higher WR than carcinoma. *1.00 group* means orbital lymphoma; *2.00 group* means orbital other malignancies
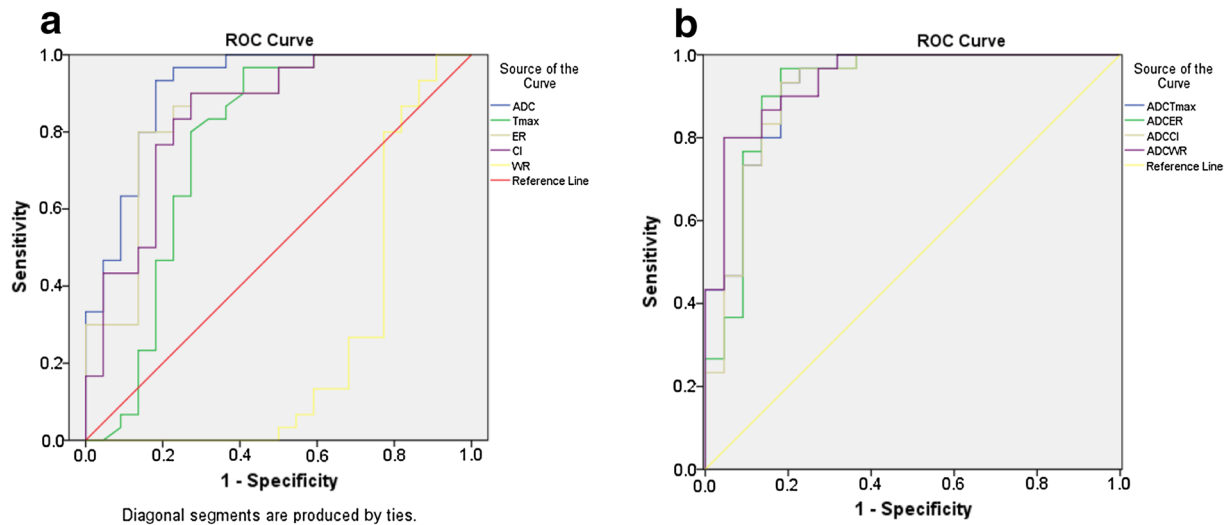
Fig. 4 a Receiver operating curve analysis comparing the diagnostic accuracy of ADC, T_{max}, ER, CI, and WR to differentiate orbital lymphoma from other malignancies. **b** Binary logistic regression and ROC analysis comparing the diagnostic accuracy of combination of DW imaging and DCE MR imaging to differentiate orbital lymphoma from other malignancies

Table 4 Relationship of index between lymphoma and other malignancies

Index	Cutoff value	AUC	95% CI	Sensitivity	Specificity	Accuracy
ADC	0.888	0.912	0.828 0.996	93.33 (28 30)	81.82 (18 22)	88.46 (46 52)
T_{max}	213.5	0.764	0.612 0.917	96.67 (29 30)	59.09 (13 22)	80.77 (42 52)
ER	1.038	0.855	0.744 0.966	80 (24 30)	86.36 (19 22)	82.69 (43 52)
CI	0.908	0.844	0.731 0.956	90 (27 30)	72.73 (16 22)	82.69 (43 52)
WR	0.046	0.750	0.590 0.910	86.67 (26 30)	68.18 (15 22)	78.85 (41 52)
ADC + T_{max}		0.923	0.846 0.999	93.33 (28 30)	81.82 (18 22)	88.46 (46 52)
ADC + ER		0.917	0.823 1.000	96.67 (29 30)	81.82 (18 22)	90.38 (47 52)
ADC + CI		0.914	0.827 1.000	93.33 (28 30)	81.82 (18 22)	88.46 (46 52)
ADC + WR		0.939	0.872 1.000	80 (24 30)	95.45 (21 22)	86.54 (45 52)

Discussion

Orbital lymphoma is the most common malignant orbital tumor in adults [8, 21], but it still poses a great clinical and radiological diagnostic challenge because its manifestation and characteristics with conventional imaging are not specific. To our knowledge, there has been no major published study on the diagnostic capabilities of DW imaging and DCE MR imaging in distinguishing lymphoma from other malignancies in the orbit. Our study found that the differences on DW imaging and DCE MR imaging were great between orbital lymphoma and other malignancies.

Our DW imaging findings of orbital lymphoma were similar to those in previous studies [8, 9, 15], which showed relatively low mean ADC values, due to their high cellularity and their high nucleus-to-cytoplasm ratio [1, 8, 9, 15, 16]. A study by Politi [8] gave mean ADC values

of orbital lymphoma of $0.666 \pm 0.073 \times 10^{-3}$ mm^2/s, whereas a study by Haradome [9] gave them as $0.54 \pm 0.05 \times 10^{-3}$ mm^2/s. The mean ADC values of orbital lymphoma were $0.711 \pm 0.152 \times 10^{-3}$ mm^2/s in Xu's study [15] and $0.694 \pm 0.128 \times 10^{-3}$ mm^2/s in our study. All of these studies [8, 9, 15, 16] demonstrated very similar distributions of orbital lymphoma ADCs. However, all of them [9, 15, 16] focused on the preoperative evaluation of the role of DW imaging in the diagnosis and management of orbital lymphoma and inflammation. Nevertheless, our study is the only one on DW imaging characteristics of orbital lymphoma and other malignancies. In previous studies [3, 7], the mean ADC values were $0.90 \pm 0.37 \times 10^{-3}$ or $0.84 \pm 0.34 \times 10^{-3}$ mm^2/s in the orbital malignant group, including lymphoma. The present study showed that, after excluding orbital lymphoma, the mean ADC values of other malignancies in the orbit were $1.186 \pm 0.315 \times 10^{-3}$ mm^2/s; also, our data

confirmed that lymphoma ($0.694 \pm 0.128 \times 10^{-3}$ mm²/s) has a significantly lower mean ADC value than that of other malignancies ($1.186 \pm 0.315 \times 10^{-3}$ mm²/s) ($P < 0.001$). Politi [8] provided a threshold of 0.775×10^{-3} mm²/s with 94.4% accuracy in distinguishing orbital lymphoma from other orbital mass lesions (including primary non-lymphoma neoplasms, benign vascular lesions, inflammatory lesions and metastases). Concentrating on DW imaging characteristics of orbital lymphoma and other malignancies, we reported an ADC cutoff value of 0.888×10^{-3} mm²/s resulting in 93.33% sensitivity, 81.81% specificity and 88.46% accuracy.

DCE MR imaging, a method offering information on physiological tissue microcirculation characteristics, provided noninvasive assessment of tumor vascularity and perfusion. In recent years, semi-quantitative and quantitative methods of DCE MR imaging have garnered increasing attention in the literature on diagnosis of orbital tumors [6, 11, 14–16]. Yuan's and Ro's studies [11, 14] showed that TIC is effective for differentiation of orbital malignant tumors from benign ones. These two studies suggested that DCE MR imaging had shown clinical utility in revealing high vascular permeability and high perfusion in orbital malignant lesions. Furthermore, our study suggested that DCE MR imaging was a valuable MR protocol for revealing different characteristics of local microcirculatory environments between lymphoma and other malignancies in the orbit. Lymphoma was associated with autoimmune disease or infection, which could explain why lymphoma had more blood vessels and higher permeability than other malignancies in the orbit. So, in our study, the T_{max}, ER, CI and WR values in patients with lymphoma were significantly different from those in patients with other orbital malignancies ($P = 0.001$, $P < 0.001$, $P < 0.001$, and $P = 0.002$, respectively), and T_{max} showed the optimal sensitivity (96.67%).

Among recent advances in MR imaging techniques, a combination of DW imaging and DCE MR imaging has improved the effectiveness of orbital MR imaging for evaluating malignant lesions [14–16]. As a result, these techniques have been increasingly used for clinical orbital MR imaging. According to Sun's study [16], a combination of DW imaging and DCE MR imaging significantly improved differentiation of orbital lymphoma from orbital inflammation, compared with DW imaging alone. With the combination of DW imaging and DCE MR imaging, our study found optimal accuracy (ADC and ER) and optimal specificity (ADC and WR) could be achieved in differentiating lymphoma from other malignancies in the orbit. In the clinical setting, the high accuracy and specificity could be valuable in detecting orbital lymphoma, which is crucial for determination of a therapy plan.

In addition to the intrinsic limits of a retrospective study, our study had several limitations. First, manual ROI measurements increased variability in a multiobserver setting and decreased intraobserver reproducibility when compared with an assisted, semiautomatic or automatic lesion measurement technique [22]. In addition, instead of the 3.2-mm section thickness without gap used in the DCE MR imaging, we used a 3-mm section thickness with a 0.3-mm gap for the DW imaging, which led to the ROI placement not being located in the same section between DW imaging and DCE MR imaging. Last, we focused on the semi-quantitative analysis of DCE-MR imaging, but quantitative assessment of k^{trans} can provide more information and improve the diagnostic efficiency of this modality.

In conclusion, DW imaging or DCE MR imaging alone was valuable for differentiation of orbital lymphoma from other malignancies. Optimal sensitivity, specificity and accuracy were yielded by combination of DW imaging and DCE MR imaging.

Compliance with ethical standards

References

1. Sepahdari AR, Aakalu VK, Setabutr P, Shiehmorteza M, Naheedy JH, Mafee MF. Indeterminate orbital masses: restricted diffusion at MR imaging with echo-planar diffusion-weighted imaging predicts malignancy. Radiology. 2010;256:554–64.

2. Tailor TD, Gupta D, Dalley RW, Keene CD, Anzai Y. Orbital neoplasms in adults: clinical, radiologic, and pathologic review. Radiographics. 2013;33:1739–58.

3. Sepahdari AR, Politi LS, Aakalu VK, Kim HJ, Razek AA. Diffusion-weighted imaging of orbital masses: multi-institutional data support a 2-ADC threshold model to categorize lesions as benign, malignant, or indeterminate. AJNR Am J Neuroradiol. 2014;35:170–5.

4. Kharod SM, Herman MP, Morris CG, Lightsey J, Mendenhall WM, Mendenhall NP. Radiotherapy in the management of orbital lymphoma: a single institution's experience over 4 decades. Am J Clin Oncol. 2015. doi:10.1097/COC.0000000000000229 (**Epub ahead of print**).

5. von Holstein SL, Coupland SE, Briscoe D, Le Tourneau C, Heegaard S. Epithelial tumours of the lacrimal gland: a clinical, histopathological, surgical and oncological survey. Acta Ophthalmol. 2013;91:195–206.

6. Xian J, Zhang Z, Wang Z, Li J, Yang B, Man F, et al. Value of MR imaging in the differentiation of benign and malignant orbital tumors in adults. Eur Radiol. 2010;20:1692–702.

7. Razek AA, Elkhamary S, Mousa A. Differentiation between benign and malignant orbital tumors at 3-T diffusion MR-imaging. Neuroradiology. 2011;53:517–22.

8. Politi LS, Forghani R, Godi C, Resti AG, Ponzoni M, Bianchi S, et al. Ocular adnexal lymphoma: diffusion-weighted MR

imaging for differential diagnosis and therapeutic monitoring. Radiology. 2010;256:565–74.

9. Haradome K, Haradome H, Usui Y, Ueda S, Kwee TC, Saito K, et al. Orbital lymphoproliferative disorders (OLPDs): value of MR imaging for differentiating orbital lymphoma from benign OPLDs. AJNR Am J Neuroradiol. 2014;35:1976–82.

10. Roshdy N, Shahin M, Kishk H, Ghanem AA, El-Khouly S, Mousa A, et al. MRI in diagnosis of orbital masses. Curr Eye Res. 2010;35:986–91.

11. Yuan Y, Kuai XP, Chen XS, Tao XF. Assessment of dynamic contrast-enhanced magnetic resonance imaging in the differentiation of malignant from benign orbital masses. Eur J Radiol. 2013;82:1506–11.

12. Fatima Z, Ichikawa T, Ishigame K, Motosugi U, Waqar AB, Hori M, et al. Orbital masses: the usefulness of diffusion-weighted imaging in lesion categorization. Clin Neuroradiol. 2014;24:129–34.

13. Zhang F, Sha Y, Qian J, Huang WH, Li XF, Wang SJ, et al. Role of magnetic resonance diffusion-weighted imaging in differentiating lacrimal masses. J Magn Reson Imaging. 2014;40:641–8.

14. Ro SR, Asbach P, Siebert E, Bertelmann E, Hamm B, Erb-Eigner K. Characterization of orbital masses by multiparametric MRI. Eur J Radiol. 2016;85:324–36.

15. Xu XQ, Hu H, Liu H, Wu JF, Cao P, Shi HB, et al. Benign and malignant orbital lymphoproliferative disorders: differentiating using multiparametric MRI at 3.0T. J Magn Reson Imaging. 2017;45:167–76.

16. Sun B, Song L, Wang X, Li J, Xian J, Wang F, et al. Lymphoma and inflammation in the orbit: diagnostic performance with diffusion-weighted imaging and dynamic contrast-enhanced MRI.

J Magn Reson Imaging. 2016. doi:10.1002/jmri **(Epub ahead of print)**.

17. Zhang Z, Shi J, Guo J, Yan F, Fu L, Xian J. Value of MR imaging in differentiation between solitary fibrous tumor and schwannoma in the orbit. AJNR Am J Neuroradiol. 2013;34:1067–71.

18. Yang BT, Wang YZ, Dong JY, Wang XY, Wang ZC. MRI study of solitary fibrous tumor in the orbit. AJR Am J Roentgenol. 2012;199:506–11.

19. Sumi M, Nakamura T. Head and neck tumours: combined MRI assessment based on IVIM and TIC analyses for the differentiation of tumors of different histological types. Eur Radiol. 2014;24:223–31.

20. Yabuuchi H, Matsuo Y, Kamitani T, Setoguchi T, Okafuji T, Soeda H, et al. Parotid gland tumors: can addition of diffusion-weighted MR imaging to dynamic contrast-enhanced MR imaging improve diagnostic accuracy in characterization? Radiology. 2008;249:909–16.

21. Shields JA, Shields CL, Scartozzi R. Survey of 1264 patients with orbital tumors and simulating lesions: the 2002 Montgomery Lecture, part 1. Ophthalmology. 2004;111:997–1008.

22. Heye T, Merkle EM, Reiner CS, Davenport MS, Horvath JJ, Feuerlein S, et al. Reproducibility of dynamic contrast-enhanced MR imaging. Part II. Comparison of intra- and interobserver variability with manual region of interest placement versus semiautomatic lesion segmentation and histogram analysis. Radiology. 2013;266:812–21.